Effects of an electron reservoir on the phase diagram of chromium alloys

R. S. Fishman
Solid State Division, Oak Ridge National Laboratory, P.O. Box 2008, Oak Ridge, Tennessee 37831-6032
*and Physics Department, North Dakota State University, Fargo, North Dakota 58105-5566**

S. H. Liu
Solid State Division, Oak Ridge National Laboratory, P.O. Box 2008, Oak Ridge, Tennessee 37831-6032
(Received 23 September 1993)

The phase diagram of chromium alloys sensitively depends on the presence of an electron reservoir. With the formation of a spin-density wave (SDW), electrons are depleted from the nested electron-hole surfaces and for a finite reservoir the chemical potential will decrease. If the power ρ of the electron reservoir were infinite, then the chemical potential would remain constant and lightly doped CrMn alloys would experience a first-order transition from an incommensurate (I) to a commensurate (C) SDW state with decreasing temperature. With a power less than about 10, the reservoir will flip the phase boundary from one side of the triple point to the other, allowing a commensurate to incommensurate transition with decreasing temperature as observed experimentally. A finite reservoir also suppresses the first-order jumps in the SDW order parameter and wave vector. When $\rho \leq 2$, the CI transition is second order for all temperatures. When $\rho > 2$, the transition is second order near the triple point but first order at lower temperatures.

I. INTRODUCTION

Because they are similar in shape and size, the electron and hole surfaces of chromium alloys can be imperfectly nested[1] by a wave vector Q. The Coulomb attraction[2–4] between electrons and holes produces a spin-density wave (SDW) with wave vector close to the nesting wave vector Q. For pure chromium, the hole octahedron is slightly larger than the electron jack. Consequently, both the nesting wave vector Q and the SDW wave vector Q' are incommensurate with the lattice. The nesting of the Fermi surfaces and the Néel temperature are enhanced by doping with manganese or rhenium, which enlarges the electron jack, and worsened by doping with vanadium,[2] which enlarges the hole octahedron.

Early experiments[5–9] on lightly doped CrMn alloys revealed a first-order transition from commensurate (C) to incommensurate (I) phases of the SDW with decreasing temperature. By contrast, the theoretical phase diagram[10] without damping and with a fixed chemical potential contains a first-order incommensurate to commensurate (IC) transition with decreasing temperature over a narrow range of doping, in disagreement with experiment. This phase diagram is drawn in the solid curves of Fig. 1 for $\rho = \infty$. As defined in Ref. 10, $T_N^* \approx 77$ meV is the fictitious Néel temperature of perfectly nested chromium without impurities. The energy z_0 is proportional to the mismatch between the electron and hole surfaces, which decreases with manganese doping and increases with vanadium doping. The quantity ρ will be defined shortly.

Two explanations have been proposed for the observed CI transition. Because scattering from impurities breaks electron-hole pairs,[3] electron damping suppresses both the SDW order parameter and the Néel temperature. Near the triple point, Nakanishi and Kasuya[11] found that sufficient damping energy Γ may flip the phase separation wave and produce a CI transition. In previous work,[10,12] we studied the effects of damping on the phase diagram, SDW order parameter, and SDW wave vector at all temperatures. In agreement with Nakanishi *et al.*, we found that electron damping does indeed favor the incommensurate over commensurate phases of the SDW. The phase diagram with $\Gamma/T_N^* = 0.3$ is given by the dashed curves

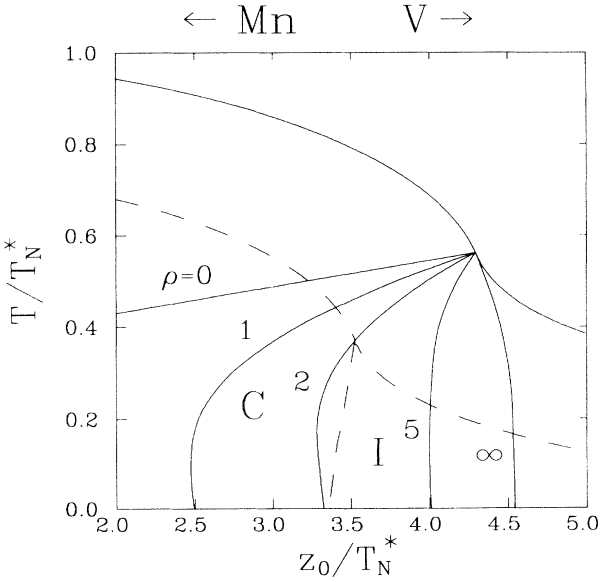

FIG. 1. The T/T_N^* vs z_0/T_N^* phase diagram of chromium alloys. The solid curves are plotted for $\Gamma = 0$ and with the indicated reservoir power. The dashed curve is plotted for $\Gamma/T_N^* = 0.3$ and $\rho = \infty$.

of Fig. 1. As well as lowering the paramagnetic phase boundary, damping also suppresses the critical value of z_0.[12] When Γ increases for a fixed z_0, the size of the drop in the SDW order parameter g at the *CI* phase boundary decreases. If Γ exceeds some critical value $\Gamma_c(z_0)$, the Néel temperature vanishes and the alloy becomes paramagnetic. About 4% impurities is required to render CrV alloys paramagnetic.[6]

Most theoretical work on chromium alloys,[3,4] including our previous studies,[10,12] implicitly assumed that the chemical potential was unaffected by the formation of the SDW and the concurrent gap $\Delta \propto g$ in the electron-hole energy spectrum. This requires an infinite reservoir of electrons, which replenishes the electron-hole band and keeps the chemical potential constant. An electron reservoir is supplied[1,13,14] by the electron balls midway between reciprocal lattice points Γ and H and by the hole pockets at N. The reservoir power ρ is just the ratio of the density of states of the reservoir band to that of the electron-hole band. But even in the absence of other bands, the nesting electron and hole surfaces centered at Γ and H may adjust to minimize any changes in the chemical potential. This violation of the rigid-band model[8] would produce an effective reservoir of unknown power.

Although several groups[11,15–19] have investigated the effects of an electron reservoir on the *CI* transition, none of these calculations is complete. While two[11,19] involve Ginzburg-Landau expansions near the triple point, two others[15,16] are zero-temperature calculations. Whereas Kotani[17] uses an interpolation technique to find the phase boundary at intermediate temperatures, only Machida and Fujita[18] attempt to completely evaluate the phase diagram. But an emphasis on higher harmonics of the SDW leads Machida and Fujita to the faulty result that the phase boundary is second order for any reservoir power. However, all of these groups do reach similar conclusions about the qualitative effects of a finite reservoir.

When the power ρ of the reservoir is finite, the chemical potential will decrease and the effective mismatch $\bar{z}_0$ between electron and hole surfaces will increase with decreasing temperature. As can be seen from the $\rho=\infty$ phase diagram, a large value of the effective mismatch $\bar{z}_0$ favors the incommensurate over the commensurate states. By inhibiting the growth of $\bar{z}_0$, the electron reservoir favors the commensurate over the incommensurate phases of the SDW. When ρ is sufficiently small, the phase boundary will flip from one side of the triple point to the other and produce the *CI* transition. But unlike damping, the reservoir does not affect the paramagnetic phase boundary or the position of the triple point.

To clarify the effects of an electron reservoir for all temperatures and to obtain the order of the *CI* phase transition, we have calculated the free energy of chromium alloys in the presence of a finite reservoir but without damping. This paper is divided into five sections. In Sec. II we derive the self-consistent equations and free energy of a chromium alloy with a finite reservoir at nonzero temperature. Section III repeats those calculations for $T=0$ and describes a method to solve the resulting self-consistent equations. In Sec. IV we present our results for the phase diagram, SDW order parameter, and SDW wave vector of chromium alloys. Finally, Sec. V contains a summary and conclusion. We also suggest an experiment which may demonstrate the importance of an electron reservoir. Expressions for the free energy are given in the Appendix.

II. FINITE-TEMPERATURE FORMALISM

Most of the unique properties of chromium alloys are produced by the nesting electron and hole bands with electron number $N_{\rm eh}$ and two-spin density of states $\rho_{\rm eh}$. All other bands are lumped into a single electron reservoir with electron number N_r and two-spin density of states ρ_r. As the chemical potential μ of the alloy decreases in response to the formation of a SDW, electrons will shift from the reservoir band into the electron-hole bands, buttressing the value of the chemical potential.

In the paramagnetic state, the change of the grand potential $\Omega(\mu)$ of the electron-hole and reservoir bands may be related to the change in the chemical potential by[18]

$$\Omega_{\rm eh}^{\rm para}(\bar{\mu})-\Omega_{\rm eh}^{\rm para}(\mu)=\frac{\partial\Omega_{\rm eh}^{\rm para}}{\partial\mu}(\bar{\mu}-\mu)+\frac{1}{2}\frac{\partial^2\Omega_{\rm eh}^{\rm para}}{\partial\mu^2}(\bar{\mu}-\mu)^2$$
$$=-N_{\rm eh}(\bar{\mu}-\mu)-\frac{1}{2}\rho_{\rm eh}(\bar{\mu}-\mu)^2 , \quad (1)$$

$$\Omega_r^{\rm para}(\bar{\mu})-\Omega_r^{\rm para}(\mu)=\frac{\partial\Omega_r^{\rm para}}{\partial\mu}(\bar{\mu}-\mu)+\frac{1}{2}\frac{\partial^2\Omega_r^{\rm para}}{\partial\mu^2}(\bar{\mu}-\mu)^2$$
$$=-N_r(\bar{\mu}-\mu)-\frac{1}{2}\rho_r(\bar{\mu}-\mu)^2 , \quad (2)$$

which assumes that the densities-of-states $\rho_{\rm eh}$ and ρ_r are independent of μ. Hence, the change in the total grand potential is

$$\Delta\Omega^{\rm para}=-N(\bar{\mu}-\mu)-\tfrac{1}{2}(\rho_r+\rho_{\rm eh})(\bar{\mu}-\mu)^2 , \quad (3)$$

where $N=N_{\rm eh}+N_r$ is the total number of electrons.

Defining the free energy through the Legendre transformation $F(N)=\Omega(\mu)+\mu N$, we find that the change in free energy produced by a shift in chemical potential is given by

$$\Delta F^{\rm para}=-\tfrac{1}{2}(\rho_r+\rho_{\rm eh})(\bar{\mu}-\mu)^2 . \quad (4)$$

So the difference in free energy between the SDW state with chemical potential $\bar{\mu}$ and the paramagnetic state with chemical potential μ is

$$\begin{aligned}\Delta F&=F^{\rm SDW}(\bar{\mu})-F^{\rm para}(\mu)\\&=F^{\rm SDW}(\bar{\mu})-F^{\rm para}(\bar{\mu})+\Delta F^{\rm para}\\&=\Delta F^{(0)}(\bar{\mu})-\tfrac{1}{2}\rho_{\rm eh}(1+\rho)(\bar{\mu}+\mu)^2 ,\end{aligned} \quad (5)$$

where $\rho=\rho_r/\rho_{\rm eh}$ is the ratio of density of states and $\Delta F^{(0)}(\bar{\mu})$ is the free energy calculated in Ref. (10) for an infinite reservoir with $\bar{\mu}$ replacing μ.

Since the free energy $F(N)$ cannot depend on μ, Eq. (5) is subject to the constraint[18]

$$\frac{\partial \Delta F}{\partial \bar{\mu}}=0 , \tag{6}$$

which can also be written

$$\rho_{\rm eh}(1+\rho)(\bar{\mu}-\mu)=\frac{\partial \Delta F^{(0)}(\bar{\mu})}{\partial \bar{\mu}} . \tag{7}$$

The reservoir power only enters this relation on the left-hand side. So when $\rho=\infty$, $\bar{\mu}=\mu$ and the chemical potential is unaffected by the SDW. More generally, $\partial \Delta F^{(0)}/\partial \bar{\mu}<0$ so the chemical potential $\bar{\mu}(T)$ is smaller than the chemical potential μ of the paramagnetic state.

The mismatch between the electron and hole surfaces in the paramagnetic regime is fixed by[4] the energy z_0. This parameter can be related to the wave vector

$$Q=\frac{2\pi}{a}(1-\delta) , \tag{8}$$

which imperfectly nests the electron and hole surfaces at the Néel temperature. For pure chromium, δ is approximately[6] 0.04 so that $Q<G/2\equiv 2\pi/a$ and the SDW is incommensurate with the lattice. If one side of the hole Fermi surface (translated by the nesting wave vector Q) is perfectly nested with the electron surface, then the other side (translated by $G-Q$) will differ by energy z_0 at the Fermi momentum, as shown in Fig. 2.

As the chemical potential decreases, the effective mismatch $\bar{z}_0$ increases. Assuming that the Fermi velocity v_F is constant, it is straightforward to show that

$$\bar{z}_0-z_0=4(\mu-\bar{\mu}) . \tag{9}$$

We emphasize that the effective mismatch and chemical potential are defined so that $\bar{z}_0(T_N)=z_0$ and $\bar{\mu}(T_N)=\mu$. Hence, Eqs. (5) and (7) can be rewritten as

$$\Delta F=\Delta F^{(0)}(\bar{z}_0)-\tfrac{1}{32}\rho_{\rm eh}(1+\rho)(\bar{z}_0-z_0)^2 , \tag{10}$$

$$\rho_{\rm eh}(1+\rho)(\bar{z}_0-z_0)=16\frac{\partial \Delta F^{(0)}(\bar{z}_0)}{\partial \bar{z}_0} . \tag{11}$$

Since $\Delta F^{(0)}(\bar{z}_0)$ increases as $\bar{z}_0$ increases and the nesting worsens, we again verify that $\bar{z}_0(T)>z_0$ and $\bar{\mu}(T)<\mu$. However, when the paramagnetic bands are perfectly nested with $z_0=0$, the effective mismatch $\bar{z}_0(T)$ vanishes and the chemical potential $\bar{\mu}(T)$ is constant for all T and ρ.

Because the mismatch $\bar{z}_0$ changes below T_N, the nesting wave vector Q depends on temperature. It is simple to show that

$$Q(T)=\frac{2\pi}{a}(1-\delta)-\frac{\bar{z}_0-z_0}{2v_F} . \tag{12}$$

Since $\bar{z}_0(T)>z_0$ and $d\bar{z}_0/dT<0$, the nesting wave vector $Q(T)$ decreases with decreasing temperature.

Generally, the wave vector $Q'(T)$ of the SDW lies between[10,12] the nesting wave vector $Q(T)$ and $G/2$. In the presence of a reservoir, the SDW wave vector must be written as

$$Q'(T)=\frac{2\pi}{a}\left\{1+\delta(\Lambda-1)\right\}+\frac{2\pi}{a}\kappa\frac{\bar{z}_0-z_0}{T_N^*}(\Lambda-1) , \tag{13}$$

where $\kappa=aT_N^*/4\pi v_F\approx 0.013$. The difference between the nesting wave vector Q and the SDW wave vector Q' is determined by $0\le\Lambda(T)\le 1$ and reflects the compromise[12] between the nesting of each side of the hole octahedron with the smaller electron jack. When $\Lambda=1$, the SDW wave vector is commensurate with the lattice; when $\Lambda=0$, the nesting and SDW wave vectors are identical. For an infinite reservoir, Λ jumps to 1 as z_0 decreases through the phase boundary.[10] As z_0 decreases in the commensurate regime, the nesting continues to improve and T_N continues to grow[12] until it reaches a maximum of T_N^* when $z_0=0$. For a finite reservoir, the suppression of the chemical potential with decreasing temperature tends to lower Q'. By maintaining the constancy of the chemical potential and $\bar{z}_0$, the reservoir opposes the growth of the second term in $Q'(T)$ with decreasing temperature.

Subject to the constraint of Eq. (11) that it be an extremum with respect to $\bar{z}_0$ or $\bar{\mu}$, the free energy must also be a minimum with respect to the SDW order parameter g and the SDW wave vector parameter Λ. So in the presence of a finite reservoir, the free energy can be written

$$\Delta F(z_0,T)=\min_{g,\Lambda}\{\sup_{z_0}[\Delta F^{(0)}(\bar{z}_0,g,\Lambda,T) - \tfrac{1}{32}\rho_{\rm eh}(1+\rho)(\bar{z}_0-z_0)^2]\} . \tag{14}$$

Since the reservoir power ρ does not enter $\Delta F^{(0)}(\bar{z}_0)$, the self-consistent solutions which minimize $\Delta F(z_0)$ need only be extrema of $\Delta F^{(0)}(\bar{z}_0)$. In fact, this set of self-consistent solutions $\{g,\Lambda\}$ may *maximize* the infinite-reservoir free energy $\Delta F^{(0)}(\bar{z}_0)$. By contrast, Angelescu, Nenciu, and Tonchev[19] define the free energy so that the minimization with respect to g and Λ precedes the extremization with respect to $\bar{z}_0$. As we shall see, the extremum condition will then have *no solution* for ranges of the energy mismatch z_0. To avoid this unphysical situation, the order of operations in Eq. (14) must be maintained.

The infinite-reservoir free energy $\Delta F^{(0)}(\bar{z}_0)$ is taken from Ref. 10 in the absence of damping[15] and is given by

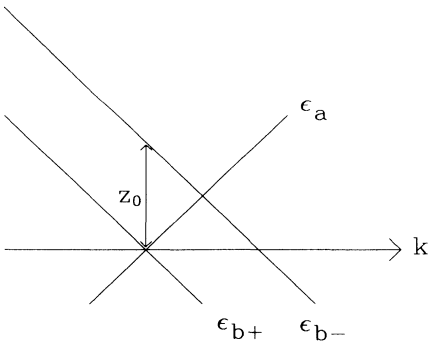

FIG. 2. The band structure of chromium when the hole surface is translated by either Q (giving energy ϵ_{b+}) or $G-Q$ (giving energy ϵ_{b-}).

Eq. (A1) in the Appendix. The self-consistent solutions for $\{g,\Lambda\}$ are obtained from the extremum conditions

$$\frac{\partial \Delta F^{(0)}(\bar{z}_0,g,\Lambda,T)}{\partial g}=0 , \tag{15a}$$

$$\frac{\partial \Delta F^{(0)}(\bar{z}_0,g,\Lambda,T)}{\partial \Lambda}=0 , \tag{15b}$$

just as in Ref. 10 except that now both minima and maxima sets of solutions are retained and tabulated as functions of $\bar{z}_0$. The extremum condition with respect to $\bar{z}_0$ is given by Eq. (11). Notice that $\bar{z}_0$ is independent of ρ_{eh} and depends only on the ratio of reservoir powers ρ.

Since $\bar{z}_0=z_0$ at the Néel temperature, the positions of the paramagnetic phase boundary and the triple point are unaffected by the power of the reservoir. However, as we shall see in Sec. IV, the *CI* phase boundary can be substantially changed by the reservoir power. To obtain the new *CI* boundary, we cannot simply translate the *IC* boundary for an infinite reservoir by the value of $\bar{z}_0-z_0$ given in Eq. (11). Because the *CI* transition is first order, the effective mismatch $\bar{z}_0$ changes discontinuously across the phase boundary and the phase diagram must be calculated by matching free energies with Eqs. (10) and (A1).

III. ZERO-TEMPERATURE FORMALISM

For an infinite reservoir, the zero-temperature free energy is again taken from Ref. 10 in the absence of damping[15] and is given by Eq. (A2) in the Appendix. Of course, the total free energy is then given by Eq. (10).

Some exact results may be derived in the commensurate phase with $\Lambda=1$. When $\rho=\infty$, the self-consistent solution for the SDW order parameter can be solved in three different regimes. If $\bar{z}_0>4t$, where $t\equiv\pi T_N^*/\gamma$, then only the trivial solution $g=0$ exists. In the range $2t<\bar{z}_0<4t$, three self-consistent solutions are possible: the trivial solution, the maximum solution g_1, and the minimum solution g_0. The nontrivial solutions are given by

$$g_0^2=\tfrac{1}{2}t^2 , \tag{16a}$$

$$g_1^2=\tfrac{1}{4}t(\bar{z}_0-2t) . \tag{16b}$$

Notice that $g_1=g_0$ when $\bar{z}_0=4t$ and that $g_1\to 0$ as $\bar{z}_0\to 2t$. Finally, when $\bar{z}_0<2t$, only the minimum solution of Eq. (16a) survives. Evaluated at g_0 and g_1, the $\rho=\infty$ free energy is given by

$$\Delta F^{(0)}(\bar{z}_0,g_0,\Lambda=1)=-\tfrac{1}{2}\rho_{eh}(g_0^2-\tfrac{1}{16}\bar{z}_0^2) , \tag{17a}$$

$$\Delta F^{(0)}(\bar{z}_0,g_1,\Lambda=1)=-\tfrac{1}{2}\rho_{eh}(g_1^2-\tfrac{1}{8}\bar{z}_0^2+\tfrac{1}{4}\bar{z}_0 t) . \tag{17b}$$

The last expression only holds in the intermediate regime $2t<\bar{z}_0<4t$ where g_1 is a valid solution.

When $\rho<\infty$, the free energy of the commensurate solutions may be constructed with Eq. (10) subject to the constraint of Eq. (11). If $\rho>1$, then g_0 has the lowest free energy in the range

$$0\le z_0<2\sqrt{2}t\sqrt{\rho/(\rho+1)}<2\sqrt{2}t\approx 4.989T_N^* . \tag{18}$$

Otherwise the paramagnetic state has lower free energy. If $\rho\le 1$, then g_0 is stable when

$$0\le z_0<4t\frac{\rho}{\rho+1} , \tag{19}$$

while g_1 is stable when

$$4t\frac{\rho}{\rho+1}<z_0<2t . \tag{20}$$

At the boundary $z_0=4t\rho/(\rho+1)$, $g_1=g_0$. So in the subspace of commensurate solutions, the minimum of $\Delta F(z_0)$ may correspond to the maximum of $\Delta F^{(0)}(\bar{z}_0)$. These results for the commensurate solutions agree with the $T=0$ calculation of Rice,[16] who used spheres to approximate the octahedral electron and hole Fermi surfaces.

Of course, the physical ground state is obtained by minimizing the free energy in the space of all possible $\{g,\Lambda\}$, not just in the subspace of commensurate solutions. Solving for the incommensurate solutions numerically, we again find both minima and maxima solutions of the infinite-reservoir free energy $\Delta F^{(0)}(\bar{z}_0,g,\Lambda)$. The minima solutions $\{g_{min},\Lambda_{min}\}$ exist in the range $4.37T_N^*\le\bar{z}_0<\infty$ and both g_{min} and Λ_{min} decrease with $\bar{z}_0$. On the other hand, the maxima solutions $\{g_{max},\Lambda_{max}\}$ exist in the smaller range $4.37T_N^*\le\bar{z}_0<2\sqrt{2}t\approx 4.989T_N^*$. Unlike g_{min} and Λ_{min}, both g_{max} and Λ_{max} are increasing functions of $\bar{z}_0$. The starting values of g and Λ are approximately $\{0.95T_N^*,0.39\}$ for both the minima and maxima solutions. But as $\bar{z}_0\to 2\sqrt{2}t$, the maximum solution merges with the minimum commensurate solution so that $\{g_{max},\Lambda_{max}\}\to\{1.248T_N^*,1\}$.

Comparing the free energies of the commensurate and incommensurate solutions, we find that the maximum commensurate solution $\{g_1,1\}$ never minimizes the total free energy. So in the commensurate phase $\{g_0,1\}$, the extremum condition with respect to $\bar{z}_0$ yields

$$\bar{z}_0=\frac{\rho+1}{\rho}z_0 . \tag{21}$$

When $\rho<2$, the commensurate solution $\{g_0,1\}$ merges with the incommensurate maximum solution $\{g_{max},\Lambda_{max}\}$ at $\bar{z}_0=2\sqrt{2}t$. Then $\{g_{max},\Lambda_{max}\}$ joins the incommensurate minimum solution $\{g_{min},\Lambda_{min}\}$ at $\bar{z}_0\approx 4.37T_N^*$. So whenever $\rho<2$, the *CI* transition is *second* order at $T=0$. The phase boundary is then given by Eq. (21) as

$$z_0^{CI}=2\sqrt{2}t\frac{\rho}{1+\rho}\approx\frac{8.886}{\gamma}\frac{\rho}{1+\rho}T_N^* , \quad \rho\le 2 . \tag{22}$$

Since z_0^{CI} vanishes as $\rho\to 0$, the incommensurate phase is stable for all $z_0>0$ at zero temperature in the absence of a reservoir.

For $\rho>2$, the commensurate solutions become unstable to the incommensurate solutions $\{g_{max},\Lambda_{max}\}$ or $\{g_{min},\Lambda_{min}\}$ for $\bar{z}_0<2\sqrt{2}t$. Hence, the *CI* transition is first order and accompanied by jumps in the effective mismatch $\bar{z}_0$ and chemical potential $\bar{\mu}$.

In the earliest study of a finite reservoir, Shibatani

et al.[15] get most of the details right. By minimizing the energy at $T=0$, they obtain a phase transition which becomes second order when $\rho<\rho_c$, where ρ_c lies between 1 and 2. When $\rho=0$, this phase transition is completely suppressed. But rather than jumping to $2\pi/a$, the SDW wave vector jumps to a slightly smaller value and only reaches $2\pi/a$ when $z_0=0$. So instead of a CI transition, Shibatani *et al.* obtain a transition between two incommensurate states, one of which gradually becomes commensurate.

Despite its success in the commensurate regime, Rice's spherical model[16] does not fare quite so well in the incommensurate regime, where the octahedral shapes of the Fermi surfaces become important. Rice finds that the $T=0$ transition becomes second order when $\rho<0.31$, a much smaller critical value than found here. He also obtains a result for $z_0^{\rm CI}$ which is $\sqrt{2}$ times larger than in Eq. (22)

While Machida and Fujita[18] agree with Rice[16] that the incommensurate ground state is stable for all z_0 when $\rho=0$, they also conclude that the *CI* transition is always second order. For any ρ, their $T=0$ boundary is given by

$$z_0^{CI}=\frac{8}{\gamma}\frac{\rho}{1+\rho}T_N^* , \tag{23}$$

which overestimates the incommensurate portion of the diagram. Part of the reason for this discrepancy may be that Machida and Fujita include higher odd harmonics in the SDW order parameter.

As mentioned above, Angelescu, Nenciu, and Tonchev[19] have suggested that the total free energy must be minimized only in the subspace of the minima solutions $\{g_0,1\}$ and $\{g_{\rm min},\Lambda_{\rm min}\}$ of the $\rho=\infty$ free energy. If this procedure is performed, then there will be a gap in z_0 between the commensurate solutions $\{g_0,1\}$ and the incommensurate solutions $\{g_{\rm min},\Lambda_{\rm min}\}$ for small ρ. Since chromium alloys can be prepared with any desired value of doping and paramagnetic mismatch z_0, such a gap has no physical interpretation. The maxima solutions $\{g_{\rm max},\Lambda_{\rm max}\}$, which minimize the total free energy of Eq. (10) subject to Eq. (11), are required to fill this gap in the phase diagram. It is also simple to show that the free energy of Angelescu, Nenciu, and Tonchev must be an upper bound on the free energy of Eq. (14).

The physical effects of a reservoir are easy to understand. Since first-order changes in the SDW order parameter g are accompanied by discontinuous changes in the population of the nested bands, an electron reservoir is required to replenish the electron-hole band. So the first-order *CI* transition is enhanced by a large reservoir and suppressed by a small one. When the power of the reservoir is too small, first-order changes in the SDW order parameter are prohibited and the *CI* transition becomes second order.

As many authors have noted,[3] there is a close relationship between the BCS theory of superconductivity and the itinerant theory of antiferromagnetism. In the commensurate regime at $T=0$, the energy gap between the two electron-hole bands (the $b-$ and $b+$ bands of Fig. 2 coalesce into a single hole band) is given by the BCS result $\Delta(0)=\sqrt{2}g(0)\approx 1.764T_N^*$, which uses Eq. (16a) for g_0. But in the incommensurate regime with $\Lambda\ll 1$, the energy gap between the a and $b+$ bands of Fig. 2 is given by $\Delta(0)=g(0)$. While the magnitude of the magnetic moment at the atomic sites is constant in the commensurate regime, it varies sinusoidally in the incommensurate regime. Consequently, the ratio $\Delta(0)/g(0)$ is smaller by a factor of $\sqrt{2}$ in the incommensurate regime.

IV. PHASE DIAGRAM, SDW ORDER PARAMETER, AND WAVE VECTOR

The finite-temperature phase boundary is calculated in the same way as described in the previous section for zero temperature. First, we tabulate all the self-consistent solutions $\{g,\Lambda\}$ of the infinite-reservoir free energy for a fixed T/T_N^*. Then for finite ρ, we compare the free energies of these solutions subject to the constraint of Eq. (11). For sufficiently small $\rho<\rho_c$, the commensurate minima solutions merge with the incommensurate maxima solutions to produce a second-order phase transition.

After numerically evaluating the *CI* phase boundary for several temperatures, we find that ρ_c is a monotonically increasing function of temperature. Calculating ρ_c for six values of T/T_N^*, we plot ρ_c versus temperature in Fig. 3. Although not proven here, we speculate that ρ_c diverges as T/T_N^* approaches the triple point value of 0.562. This would imply that the *CI* transition is always second order sufficiently close to the triple point. However, the steep increase in Λ near the second-order transition at high temperatures may easily be mistaken for a first-order transition.

In Fig. 1, we plot the phase diagram of chromium alloys for several values of ρ. Because it increases the effective mismatch $\bar{z}_0$, a small reservoir enhances the in-

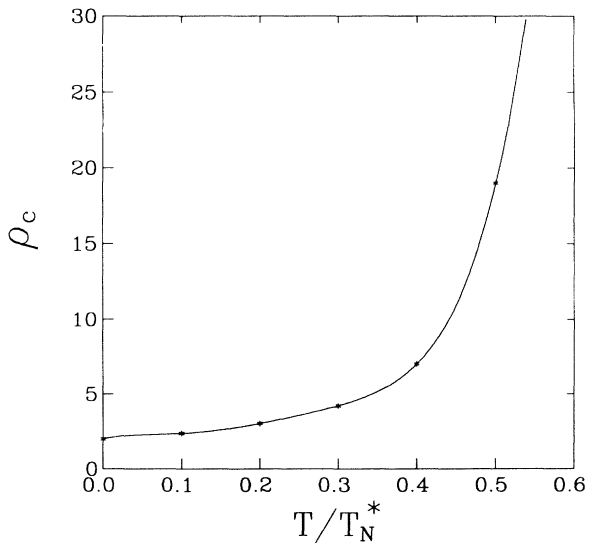

FIG. 3. The critical value ρ_c, below which the *CI* transition is second order, vs T/T_N^* for six values of T/T_N^* and a fitted curve.

commensurate portion of the phase diagram. For any value of ρ smaller than about 10, the phase boundary flips from the right to the left of the triple point, producing a *CI* transition. Since the reservoir power is almost certainly less than 10, we conclude that damping is not needed to explain the *CI* transition. However, damping is required to understand the behavior of the SDW wave vector and order parameter when chromium is doped with isoelectronic impurities like molybdenum or tungsten.[6,11]

The phase diagram of Fig. 1 is qualitatively similar to that of Machida and Fujita,[18] except that the latter slightly overestimate the incommensurate portion of the phase diagram and obtain second-order transitions throughout. This phase diagram also agrees qualitatively with the Ginzburg-Landau expansion of Nakanishi and Kasuya,[11] who include both damping and a finite reservoir. For large reservoirs, damping pulls the phase boundary to the left and favors the incommensurate phase. But for $\rho=0$, Nakanishi *et al.* find that damping pulls the phase boundary to the right and favors the commensurate phase. So the incommensurate portion of the phase diagram is largest when both ρ and Γ vanish. Nakanishi *et al.* also investigate the different effects of normal and magnetic impurities on the incommensurate-normal phase boundary.

Using an interpolation technique between large and small z_0, Kotani[17] (previously called Shibatani) found that for $\rho=0$, the phase boundary bends upwards towards higher temperatures before falling back down to intercept zero temperature at $z_0=0$. This upwards bulge persists until ρ is between 1 and 2. Kotani continues to find a transition between two incommensurate regimes, one of which becomes commensurate only gradually as $z_0\to 0$.

The slight bulge of the *CI* phase boundaries to the left in Fig. 1 would seem to permit a *CIC* transition with decreasing temperature. This bulge is most noticeable for intermediate values of ρ near 2 but is present for all nonzero values of ρ which allow a *CI* transition. However, we believe that even a small amount of damping will wipe out the bulge and eliminate the possibility of a *CIC* transition.

In Fig. 4, we plot the $T=0$ SDW order parameter $g(0)$ versus z_0 for several values of ρ. The first-order jump in $g(0)$ can be clearly seen for $\rho=\infty$ and 5. For $\rho\leq 2$, the *CI* transition is second order and $g(0)$ changes continuously. When $\rho=0$, $g(0)$ does not reach its commensurate value of $t/\sqrt{2}\approx 1.248T_N^*$ until $z_0=0$. As z_0/T_N^* increases above 5 or so, $g(0)/T_N^*$ becomes relatively insensitive to the power of the reservoir.

To plot the results for the SDW wave vector, we define the parameter $\bar{\Lambda}$ by

$$\bar{\Lambda}=\Lambda+\frac{\kappa}{\delta}\frac{\bar{z}_0-z_0}{T_N^*}(\Lambda-1)\,, \tag{24}$$

so that the SDW wave vector is given by

$$Q'(T)=\frac{2\pi}{a}\{1+\delta(\bar{\Lambda}-1)\}\,. \tag{25}$$

Unlike $\Lambda>0$, $\bar{\Lambda}$ may be negative. In the following plots, we set $\kappa/\delta=\frac{1}{3}$.

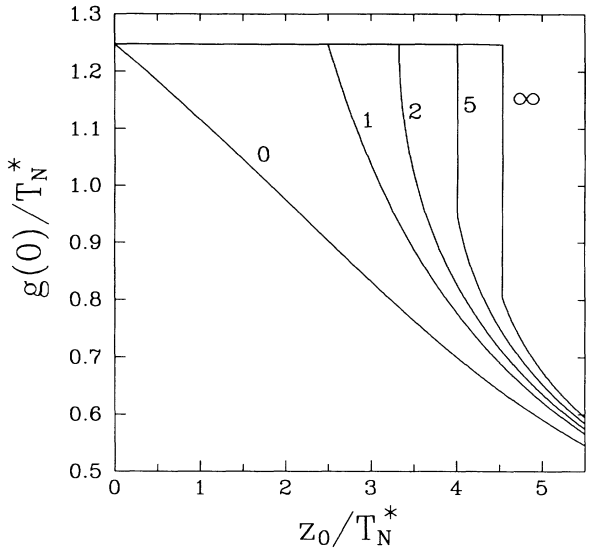

FIG. 4. The normalized $T=0$ SDW order parameter vs z_0/T_N^* for different values of ρ.

At $T=0$, $\bar{\Lambda}(0)$ is plotted in Fig. 5. The first-order jump in $\bar{\Lambda}(0)$ decreases as ρ decreases until, for $\rho\leq 2$, the *CI* transition and $\bar{\Lambda}(0)$ are continuous. For small values of ρ, $\bar{\Lambda}(0)$ may become negative in some range of z_0/T_N^*. A negative value for $\bar{\Lambda}$ implies that the zero-temperature SDW wave vector $Q'(0)$ is smaller than the nesting wave vector $Q(T_N)$ evaluated at T_N. However, at any temperature T, the SDW wave vector $Q'(T)$ always lies between $G/2$ and the nesting wave vector $Q(T)$ evaluated at the same temperature.

In Fig. 6, we plot the difference between the $T=0$ mismatch energy $\bar{z}_0$ and the paramagnetic mismatch z_0, both normalized by T_N^*. Since $\bar{z}_0-z_0=4(\mu-\bar{\mu})$, Fig. 6

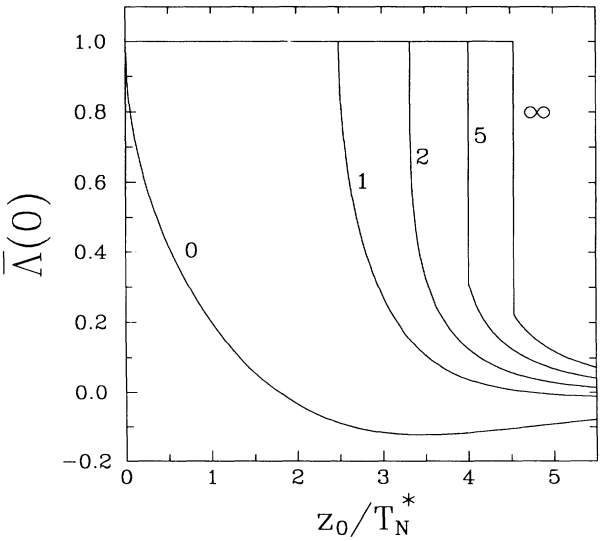

FIG. 5. The $T=0$ wave-vector parameter $\bar{\Lambda}$ vs z_0/T_N^* for different values of ρ.

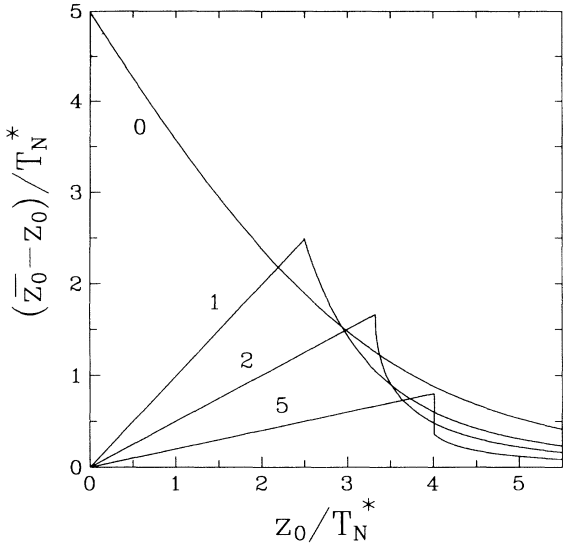

FIG. 6. The $T=0$ difference $\bar{z}_0 - z_0$ normalized by T_N^* vs z_0/T_N^* for different values of ρ.

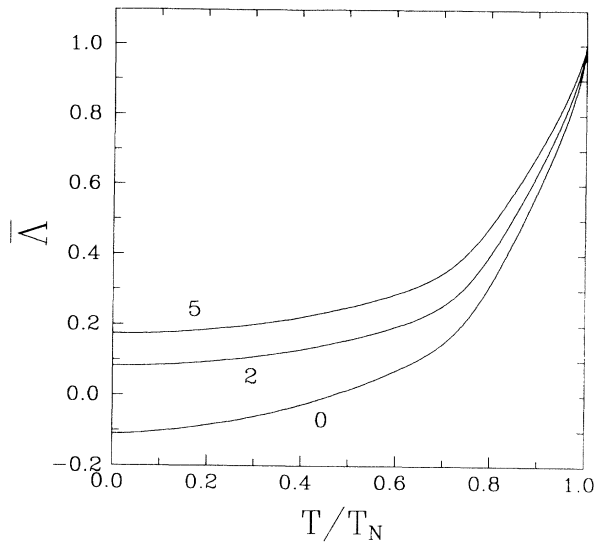

FIG. 8. The wave-vector parameter $\bar{\Lambda}$ vs T/T_N for $z_0/T_N^*=4.28$ and different values of ρ.

can also be interpreted as a plot of the chemical potential versus doping at zero temperature. When $\rho=\infty$ (not drawn), $\bar{z}_0=z_0$ and the chemical potential is constant. For finite values of ρ larger than 2, $\bar{z}_0$ increases discontinously as z_0 decreases through the *CI* transition. So as the SDW order parameter jumps up with Mn or Re doping,[8] the chemical potential must jump down to keep the particle number constant. For $\rho \leq 2$, the *CI* transition is second order and $\bar{z}_0$ is continuous. Note from Eq. (21) that $\bar{z}_0 - z_0 = z_0/\rho$ for any ρ below the *CI* transition. When $\rho \leq 2$, Eq. (22) indicates that $\bar{z}_0 \approx 4.989 T_N^*$ at the *CI* transition. If $\rho=0$, the incommensurate phase is always stable and $\bar{z}_0 - z_0$ is a monotonically decreasing function of z_0.

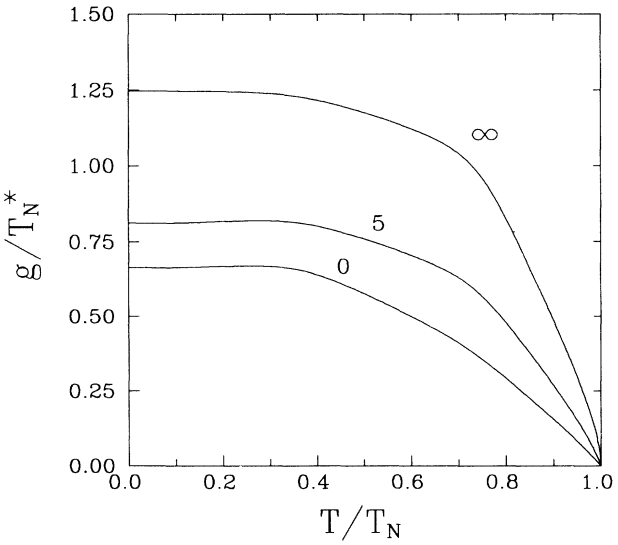

FIG. 7. The normalized SDW order parameter vs T/T_N for $z_0/T_N^*=4.28$ and different values of ρ.

While the method outlined above and in Sec. III only works for a fixed T/T_N^*, we can still learn about the temperature dependence of the SDW order parameter and wave vectors by fitting our results to a power law. If z_0/T_N^* is set to the triple point value of 4.28, then $g(T)$ and $\bar{\Lambda}(T)$ are plotted in Figs. 7 and 8. At $T=0$, the commensurate phase is stable for ρ larger than about 10, so g/T_N^* then assumes its maximum value of $\pi/\gamma\sqrt{2} \approx 1.248$. Of course, $\bar{\Lambda}$ approaches 1 for all ρ as $T \to T_N$ at the triple point. As shown, both $\bar{\Lambda}$ and g/T_N^* are monotonic functions of ρ for any fixed T/T_N.

V. CONCLUSIONS AND DISCUSSION

The earliest measurements[5–9] of the *CI* transition in chromium alloys revealed a first-order transition characterized by hysteresis but also by a large temperature width between the two phases. Some workers[7,21] speculated that the commensurate and incommensurate rate phases may coexist in certain ranges of the phase diagram. Latter, more precise measurements[22] confirmed the first-order nature of the transition and revealed that the large width of the transition regime in earlier measurements was caused by inhomogeneities in the experimental samples.

In this paper, we have studied the *CI* transition in the presence of an electron reservoir, which can replenish the electrons lost by the electron-hole bands during the formation of the SDW. The present work suggests that whenever ρ is finite, the *CI* phase transition will become second order sufficiently close to the triple point. Experiments[5–9,21,22] on the *CI* transition have been performed far enough away from the triple point that the observed transition is always first order. While it would be interesting to test this prediction closer to the triple point, first-order jumps in the order parameter and wave vector may be difficult to distinguish from second-order changes

in this regime.

Since the observed *CI* phase transition[8] is strongly first order at low temperatures and occurs within a narrow window of manganese concentrations, we estimate that ρ lies between 3 and 7. Such a large reservoir may not be provided by the extra electron and hole pockets in the band structure.[13,14] For pure chromium, Asano and Yamashita[13] find that the total density of states ρ_t decreases from 12.1/atom Ry in the paramagnetic state to 8.6/atom Ry in the incommensurate SDW state. If we attribute this difference to *half* the electron-hole density of states, then $\rho_{eh}=7.0$/atom Ry, $\rho_r=\rho_t-\rho_{eh}=5.1$/atom Ry, and $\rho\approx 0.73$, which is much too small to account for the observed phase diagram. We note that other authors[11,18] obtained a much higher value of $\rho=2.4$ after underestimating ρ_{eh} by half.

While the extra pockets in the band structure may not provide an adequate electron reservoir, the nested electron-hole band may itself oppose changes of the chemical potential and provide an effective reservoir of electrons. Since the dependence of the band structures on magnetic ordering is poorly understood,[8] we cannot estimate ρ more quantitatively.

Because the theoretical phase diagram is constructed in terms of the energy mismatch z_0 of the paramagnetic state, experimental measurements of this quantity are rather important. Using optical reflectivity measurements, Lind and Stanford[23] estimated that $z_0\approx 450$ meV for pure chromium. But the dramatic effects of doping pure chromium with a small amount of manganese or vanadium conflict[12] with such a large estimate of z_0, which is too far above the triple point. However, the measurements of Lind and Stanford actually yield the effective mismatch $\bar{z}_0$ at low temperatures rather than the paramagnetic mismatch z_0 at T_N. We see from Fig. 6 that if $\rho=5$, the effective mismatch $\bar{z}_0$ for pure chromium (just above the triple point) exceeds z_0 by about 10%. So the paramagnetic mismatch probably lies closer to 400 meV, in better agreement with other indications.

To conclude, we have investigated the effects of damping and an electron reservoir on the phase diagram of chromium alloys. While either sufficiently strong damping or a sufficiently small reservoir can explain the *CI* transition, we believe that a combination of the two is required to explain the detailed phase boundary. Experiments close to the triple point may reveal second-order *CI* transitions and confirm the importance of a finite electron reservoir.

ACKNOWLEDGMENTS

We would like to acknowledge support from the U. S. Department of Energy under Contract No. DE-AC0584OR21400 with Martin Marietta Energy Systems, Inc. Useful conversations with J. F. Cooke and B. Sternlieb are also gratefully acknowledged.

APPENDIX

The expressions given below for the free energy were derived by the authors in Ref. 10. When $\rho=\infty$ and $T>0$, the free energy is given by

$$\Delta F^{(0)}(\bar{z}_0,g,\Lambda,T)=\rho_{eh}g^2\ln\left[\frac{T}{T_N^*}\right]-\rho_{eh}\sum_{n=0}^{\infty}\left\{T\int_{-\infty}^{\infty}dz\,\ln\left|1-g^2\frac{2i\omega_n-\bar{z}_0+2z}{(i\omega_n-z)[(i\omega_n-\bar{z}_0/2+z)^2-(\bar{z}_0(\Lambda-1)/2)^2]}\right|-g^2\frac{1}{n+1/2}\right\}, \tag{A1}$$

where $\omega_n=(2n+1)\pi T$ are the Matsubara frequencies.

When $\rho=\infty$ and $T=0$, the free energy is given by

$$\Delta F^{(0)}(\bar{z}_0,g,\Lambda,T=0)=\tfrac{1}{2}\rho_{eh}g^2\left\{\ln\left[\frac{\bar{z}_0^2}{T_N^{*2}}\Lambda(2-\Lambda)\right]+2\ln\left[\frac{\gamma}{\pi}\right]\right\}-\frac{\rho_{eh}}{2\pi}\int_{-\infty}^{\infty}dz\int_0^{\infty}dv\left\{\ln\left|1-g^2\frac{2iv-\bar{z}_0+2z}{(iv-z)\{(iv-\bar{z}_0/2+z)^2-[\bar{z}_0(\Lambda-1)/2]^2\}}\right|+g^2\mathrm{Re}\left[\frac{2iv-\bar{z}_0+2z}{(iv-2)\{(iv-\bar{z}_0/2+z)^2-[\bar{z}_0(\Lambda-1)/2]^2\}}\right]\right\}, \tag{A2}$$

where $\ln\gamma\approx 0.577$ is Euler's constant.

---

*Permanent address.

[1]T. L. Loucks, Phys. Rev. **139**, A1181 (1965).
[2]D. Jerome, T. M. Rice, and W. Kohn, Phys. Rev. **158**, 462 (1967).
[3]J. Zittartz, Phys. Rev. **164**, 575 (1967).
[4]C. Y. Young and J. B. Sokoloff, J. Phys. F **4**, 1304 (1974).
[5]Y. Hamaguchi, E. O. Wollan, and W. C. Koehler, Phys. Rev. **138**, A737 (1965).

[6]W. C. Koehler, R. M. Moon, A. L. Trego, and A. R. Mackintosh, Phys. Rev. **151**, 405 (1966).
[7]T. J. Bastow, Proc. Phys. Soc. **88**, 935 (1966)
[8]S. Komura, Y. Hamaguchi, and N. Kunitomi, J. Phys. Soc. Jpn. **23**, 171 (1967).
[9]Y. Syono and Y. Ishikawa, Phys. Rev. Lett. **19**, 747 (1967).
[10]R. S. Fishman and S. H. Liu, Phys. Rev. B **48**, 3820 (1993).
[11]K. Nakashini and T. Kasuya, J. Phys. Soc. Jpn. **42**, 833 (1977).
[12]R. S. Fishman and S. H. Liu, Phys. Rev. B **47**, 11 870 (1993).
[13]S. Asano and J. Yamashita, J. Phys. Soc. Jpn. **23**, 714 (1967).
[14]J. Rath and J. Callaway, Phys. Rev. B **8**, 5398 (1973).
[15]A. Shibatani, K. Motizuki, and T. Nagamiya, Phys. Rev. **177**, 984 (1969).
[16]T. M. Rice, Phys. Rev. B **2**, 3619 (1970).
[17]A. Kotani, J. Phys. Soc. Jpn. **36**, 103 (1979).
[18]K. Machida and M. Fujita, Phys. Rev. B **30**, 5284 (1984).
[19]N. Angelescu, G. Nenciu, and N. S. Tonchev, Phys. Lett. **93A**, 201 (1983); J. Phys. F **14**, 2155 (1984).
[20]Actually the free energy of Ref. 10 must be multiplied by ρ_{eh}/λ so that it correctly reduces to the BCS result $\Delta F=-\rho_{eh}g^2/2$ in the $T=0$ commensurate limit.
[21]E. I. Kondorsky, T. I. Kostina, and V. Yu. Galkin, *Transition Metals, 1977,* edited by M. J. G. Lee, J. M. Perez, and E. Fawcett (Institute of Physics, Bristol, 1978), p. 611.
[22]B. M. Geerken, R. Griessen, G. Benediktsson, H. U. Astrom, and C. van Dijk, J. Phys. F **12**, 1603 (1982).
[23]M. A. Lind and J. L. Stanford, Phys. Lett. **39A**, 5 (1972).